JOURNAL OF CATALYSIS **173,** 196–209 (1998)
ARTICLE NO. CA971907

Partially Decarbonylated Tetrairidium Clusters on γ-Al_2O_3: Structural Characterization and Catalysis of Toluene Hydrogenation

O. Alexeev, G. Panjabi, and B. C. Gates

Department of Chemical Engineering and Materials Science, University of California, Davis, California 95616

Received June 3, 1997; revised September 12, 1997; accepted September 15, 1997

Supported metal clusters were prepared as $[Ir_4(CO)_{12}]$ was adsorbed intact from *n*-pentane solution onto γ-Al_2O_3 powder that had been partially dehydroxylated *in vacuo* at 400°C. The supported clusters were characterized by infrared spectroscopy and extended X-ray absorption fine structure (EXAFS) spectroscopy. The supported $[Ir_4(CO)_{12}]$, which was stable after heating in He at temperatures up to 100°C, was decarbonylated to various degrees by treatment in He at temperatures higher than 100°C, with the decarbonylation being complete at 300°C. EXAFS data indicated an average Ir–Ir first-shell coordination number of about 3.0 at an average bond distance 2.67 Å at each stage of the decarbonylation, demonstrating that the decarbonylation proceeded without disruption of the tetrahedral cluster frame, ultimately giving Ir_4/γ-Al_2O_3. Chemisorption of hydrogen on the supported Ir_4 clusters was characterized by an H/Ir atomic ratio of about 0.13, a value much less than that characteristic of larger iridium clusters, which indicates that the supported clusters have reactivities different from those of bulk metallic iridium or iridium particles large enough to have bulklike properties. The $[Ir_4(CO)_{12}]$ clusters were partially reconstructed from Ir_4/γ-Al_2O_3 by treatment in CO at 150–200°C. The supported tetrairidium clusters at various stages of decarbonylation were found to be catalytically active for toluene hydrogenation at 60°C and atmospheric pressure. The catalytic activity of supported $[Ir_4(CO)_{12}]$ was negligible, and the activity increased with increasing decarbonylation, until the degree of decarbonylation reached about 70%, whereupon the catalytic reaction rate became almost independent of the degree of decarbonylation. The data suggest that the last remaining CO ligands have almost no effect on the toluene hydrogenation reaction because the clusters have attained a sufficient degree of unsaturation to provide bonding sites for the reactant ligands.

INTRODUCTION

Metals are among the most important catalysts, usually being applied in the form of clusters or particles dispersed on porous supports. The smaller the clusters or particles, the larger the fraction of metal atoms exposed at a surface and accessible to reactants and available for catalysis. Conventional preparation techniques result in nonuniform supported metal particles, making it difficult to characterize the metal structurally and to determine structure–catalytic property relationships. Consequently, researchers have worked with structurally defined metal catalysts—single crystals—and these are the best understood metal catalysts. However, single-crystal surfaces differ in reactivity and catalytic properties from extremely small supported metal clusters or particles (1), and there is a clear motivation for investigation of metal catalysts that are both highly dispersed and structurally uniform.

Only few supported metals with nearly uniform and well-defined structures have been made. A fruitful synthesis technique involves the use of supported molecular metal carbonyl clusters as precursors, and when these can be decarbonylated with retention (or near retention) of their metal frames, they are well suited to determination of structure–catalytic property relationships (2). For example, $[HIr_4(CO)_{11}]^-$ and $[Ir_6(CO)_{15}]^{2-}$ were used as precursors to prepare nearly uniform clusters approximated as Ir_4 and Ir_6 on MgO (3–5) and NaY zeolite (3, 6). A family of such samples is beginning to allow determination of the separate effects of the support, the metal cluster size, and the identity of the metal (3).

The prospect that supported metal carbonyl cluster precursors can be decarbonylated to various degrees with the metal frames intact offers an opportunity to determine how the carbonyl ligands affect the catalytic activity. Thus, the goal of the research described here was to investigate the decarbonylation and recarbonylation of supported $[Ir_4(CO)_{12}]$ on γ-Al_2O_3 and the effects of the carbonyl ligands on the catalytic activity of the clusters for a simple test reaction, the hydrogenation of toluene. Infrared spectroscopy, extended X-ray absorption fine-structure (EXAFS) spectroscopy, and chemisorption were used to characterize the catalysts.

EXPERIMENTAL

Methods and materials. All syntheses and sample transfers were performed with exclusion of air and moisture on

0021-9517/98 $25.00

a double-manifold Schlenk line and in a N_2-filled Braun glovebox. N_2 and He (Matheson, 99.999%) were purified by passage through traps containing particles of Cu and activated zeolite to remove traces of O_2 and moisture, respectively. *n*-Pentane (Aldrich), used as a solvent, and tetrahydrofuran (THF, Fisher), used in the extraction of surface species, were each refluxed under N_2 in the presence of Na/benzophenone ketyl to remove traces of water and deoxygenated by sparging of dry N_2 prior to use.

The γ-Al_2O_3 support was prepared by first forming a paste of porous γ-Al_2O_3 (Degussa, Aluminum Oxide C) and deionized water, followed by overnight drying at 120°C, calcination at 400°C in flowing O_2 (Matheson Extra Dry Grade) for 2 h, and evacuation at 10^{-3} Torr and the final temperature for 14 h. The BET surface area of the resultant material was measured to be about 100 m^2/g.

Preparation of γ-Al_2O_3-supported $[Ir_4(CO)_{12}]$. The γ-Al_2O_3-supported sample was prepared by slurrying $[Ir_4(CO)_{12}]$ with γ-Al_2O_3 powder in *n*-pentane under N_2 for 12 h at room temperature followed by overnight evacuation at 25°C to remove the solvent. $[Ir_4(CO)_{12}]$ was added in an amount sufficient to give samples containing 1 wt% Ir; because the solvent was removed, this was the Ir content of each catalyst.

Decarbonylation and recarbonylation of supported clusters. The samples were decarbonylated by treatment in flowing He as the temperature was ramped (3°C/min) from 25°C to the desired temperature and then held at that temperature for 2 h. The infrared spectrum was monitored throughout the decarbonylation process. After complete decarbonylation of the supported iridium carbonyl clusters in flowing He at 300°C, CO flow was initiated with the sample held in the cell at 25°C. The recarbonylation process was monitored by infrared spectroscopy; the sample was scanned repeatedly until no further changes in the spectrum were observed. Then the sample was heated in flowing CO as the temperature was ramped at 3°C/min from 25 to 150°C (or 200°C) and held at the final temperature for 8 h. Infrared spectra were recorded after the sample had been cooled to room temperature.

Infrared spectroscopy. Spectra were recorded with a Bruker IFS-66V spectrometer with a spectral resolution of 4 cm^{-1}. Samples were pressed into self-supporting wafers and mounted in the cell in the drybox. Each sample was scanned 64 times, and the signal was averaged.

Chemisorption of hydrogen. An RXM-100 multifunctional catalyst testing and characterization system (Advanced Scientific Designs, Inc.) with a vacuum capability of 10^{-8} Torr was used for chemisorption measurements. Samples in the glovebox were loaded into a U-shaped quartz reactor, which was closed to prevent contamination of the sample as it was transferred to the instrument. Prior to chemisorption measurements, each sample was treated in flowing He as the temperature was ramped at a rate of 3°C/min and held at the designated temperature for 2 h. The sample was then evacuated (10^{-7} Torr) at the elevated temperature and finally cooled to 25°C. Adsorption isotherms were measured at 25°C and pressures in the range 10–200 Torr. The amount of hydrogen irreversibly chemisorbed on the sample was measured as the difference between the total adsorption and the physical adsorption isotherms (two isotherms measured consecutively with 30 min of evacuation between measurements). Accuracy in H/Ir ratio determination was ±10%.

Catalytic reaction experiments. Toluene hydrogenation was performed in a once-through flow reactor at 60°C and atmospheric pressure. Prior to reaction, the catalyst samples were treated in He as the temperature was ramped (3°C/min) to the desired value (in the range 100–400°C) and held for 2 h. An Isco liquid metering pump (Model No. 260D) was used to feed the liquid toluene to the vaporization chamber, where it was mixed with H_2. The toluene and H_2 partial pressures were 50 and 710 Torr, respectively, at the reactor inlet. An on-line gas chromatograph equipped with a flame ionization detector was used to analyze the catalytic reaction products. Conversions of toluene were less than 1%. There was no measurable conversion of toluene in the absence of catalyst. Accuracy in the determination of reaction rates from differential conversions was ±10%.

EXAFS spectroscopy. EXAFS experiments were performed at X-ray beamline 2-3 at the Stanford Synchrotron Radiation Laboratory (SSRL), Stanford Linear Accelerator Center, Stanford, California, and at beamline X-11A at the National Synchrotron Light Source (NSLS), Brookhaven National Laboratory, Upton, New York. The storage ring at SSRL operated with an electron energy of 3 GeV; the ring current was 60–100 mA. The ring current at NSLS was at least 110 mA, and the ring energy was 2.5 GeV.

γ-Al_2O_3-supported iridium clusters were characterized by EXAFS spectroscopy. Samples were characterized after adsorption of $[Ir_4(CO)_{12}]$ on γ-Al_2O_3 and after various degrees of decarbonylation of the resultant surface-bound iridium carbonyl clusters. Each powder sample was pressed into a wafer with a C-clamp in a N_2-filled glovebox at SSRL or NSLS. The sample mass was calculated to give an absorbance of about 2.5 at the Ir L_{III} absorption edge. After each sample had been pressed, it was loaded into an EXAFS cell (7), sealed under a positive N_2 pressure, and removed from the drybox. The sample was then treated in flowing purified He while being heated to a temperature in the range 100–400°C at a rate of 3°C/min and held at the desired temperature for 2 h, cooled to room temperature in a flow of He, evacuated to 10^{-5} Torr, and aligned in the X-ray beam.

TABLE 1

Crystallographic Data Characterizing the Reference Compounds and Fourier Transform Ranges Used in the EXAFS Data Analysis[a]

	Crystallographic data			Fourier transform		
Sample	Shell	N	R (Å)	Δk (Å^{-1})	Δr (Å)	n
Pt foil	Pt–Pt	12	2.77	1.9–19.8	1.9–3.0	3
$Na_2Pt(OH)_6$	Pt–O	6	2.05	1.4–17.7	0.5–2.0	3
$[Ir_4(CO)_{12}]$	Ir–C	3	1.87	2.8–16.5	1.1–2.0	3
	Ir–O*	3	3.01	2.8–16.5	2.0–3.3	3
IrAl alloy	Ir–Al[b]	8	2.58	2.7–12.0	1.0–3.0	3

[a] Notation: N, coordination number for absorber–backscatterer pair; R, distance; Δk, limits used for forward Fourier transformation (k is the wavevector); Δr, limits used for shell isolation (r is distance); n, power of k used for Fourier transformation.

[b] After subtraction of Ir–Ir contributions: $N = 6$, $r = 2.98$ Å, $\Delta\sigma^2 = -0.001$ Å^2 ($\Delta\sigma^2$ is the Debye–Waller factor), $\Delta E_0 = -3.3$ eV (ΔE_0 is the inner potential correction). A theoretical Ir–Al EXAFS function was calculated with the FEFF program (44) and adjusted to agree with limited Ir–Al reference data obtained as described above for use of a larger interval in k space for fitting the iridium data (45).

The EXAFS data were recorded in the transmission mode after the cells had been cooled to nearly liquid nitrogen temperature. The data were collected with a double-crystal monochromator [Si(220) at SSRL or Si(111) at NSLS] which was detuned 15% to minimize the effects of higher harmonics in the X-ray beam. The samples were scanned at energies near the Ir L_{III} absorption edge (11,215 eV).

EXAFS reference data. The EXAFS data were analyzed with experimentally determined reference files obtained from EXAFS data characterizing materials of known structure. The Ir–Ir and Ir–$O_{support}$ interactions were analyzed with phase shifts and backscattering amplitudes obtained from EXAFS data characterizing platinum foil and $Na_2Pt(OH)_6$, respectively. The transferability of the phase shifts and backscattering amplitudes characterizing platinum and iridium (which are near neighbors in the Periodic Table) has been justified experimentally (8, 9). The Ir–C and Ir–O* contributions (where O* represents carbonyl oxygen) were analyzed with phase shift and backscattering amplitudes obtained from EXAFS data characterizing crystalline $[Ir_4(CO)_{12}]$, which has terminal and no bridging CO ligands. The parameters used to extract these results from the EXAFS data are summarized in Table 1.

EXAFS DATA ANALYSIS

The EXAFS data were extracted from the spectra with the XDAP software (10). The EXAFS function characterizing each sample was obtained from the X-ray absorption spectrum by a cubic spline background subtraction and normalized by dividing the absorption intensity by the height of the absorption edge. The final normalized EXAFS function characterizing each sample was obtained from the average of six scans. The main contributions to the spectra were isolated by inverse Fourier transformation of the final EXAFS function. The analysis was done with the Fourier-filtered data.

The parameters characterizing both low-Z (O, C) and high-Z (Ir) contributions were determined by multiple-shell fitting in r space (where r is the distance from the absorbing atom, Ir) and in k space (k is the wavevector) with application of k^1 and k^3 weighting in the Fourier transformations. The fit was optimized by use of the difference file technique (11, 12) with phase- and amplitude-corrected Fourier transforms.

RESULTS

Infrared spectra: interaction of $[Ir_4(CO)_{12}]$ with γ-Al_2O_3 and decarbonylation. After $[Ir_4(CO)_{12}]$ had been slurried overnight with γ-Al_2O_3 powder in n-pentane and the mixture had been evacuated to remove the solvent, the resultant solid powder was beige. No substantial changes in the infrared spectrum in the ν_{OH} or carbonate regions were observed for the powder relative to the spectrum of γ-Al_2O_3. New bands were observed in the ν_{CO} region (Fig. 1, spectrum 1). Those at 2112, 2072, 2062, 2029, and 2002 cm^{-1} are assigned as ν_{CO} bands of supported $[Ir_4(CO)_{12}]$, in agreement with those reported (13).

$[Ir_4(CO)_{12}]$ was extracted from the γ-Al_2O_3 surface by THF at room temperature, giving a solution spectrum with

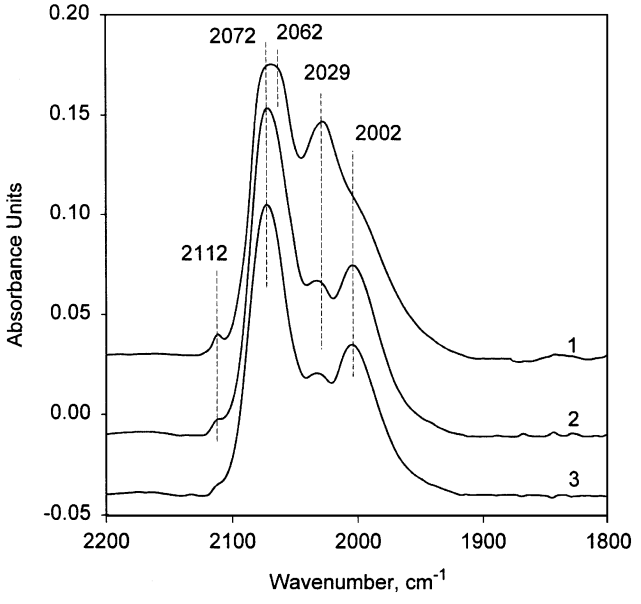

FIG. 1. Infrared spectra in the ν_{CO} region. (1) Spectrum of freshly prepared sample formed by contacting of γ-Al_2O_3 with $[Ir_4(CO)_{12}]$ in n-pentane; spectrum recorded after recarbonylation of γ-Al_2O_3-supported $[Ir_4(CO)_{12}]$ cluster previously decarbonylated in He flow at 300°C. (2) After recarbonylation in CO flow at 200°C for 8 h. (3) After recarbonylation in CO flow at 150°C for 8 h.

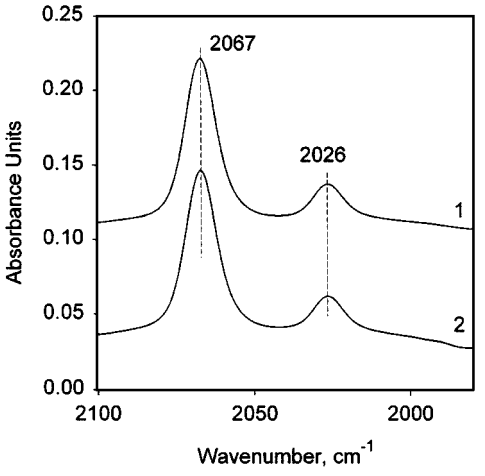

FIG. 2. Infrared spectra in the ν_{CO} region characterizing extract solutions. (1) Solution formed after contacting of freshly prepared γ-Al_2O_3-supported $[Ir_4(CO)_{12}]$ with THF. (2) Solution formed when γ-Al_2O_3-supported $[Ir_4(CO)_{12}]$ was treated in He at 100°C followed by contacting with THF.

bands at 2067 and 2026 cm^{-1} (Fig. 2, spectrum 1), which is typical for $[Ir_4(CO)_{12}]$ in THF.

Figures 3 and 4 show infrared spectra in the ν_{CO} region recorded during the decarbonylation of γ-Al_2O_3-supported $[Ir_4(CO)_{12}]$ in flowing He. Ramping the temperature to 100°C did not lead to a measurable decrease in the total absorption in the ν_{CO} region, but it did lead to changes in the relative intensities of the bands in this region. The bands at 2062 and 2002 cm^{-1} were more clearly evident in

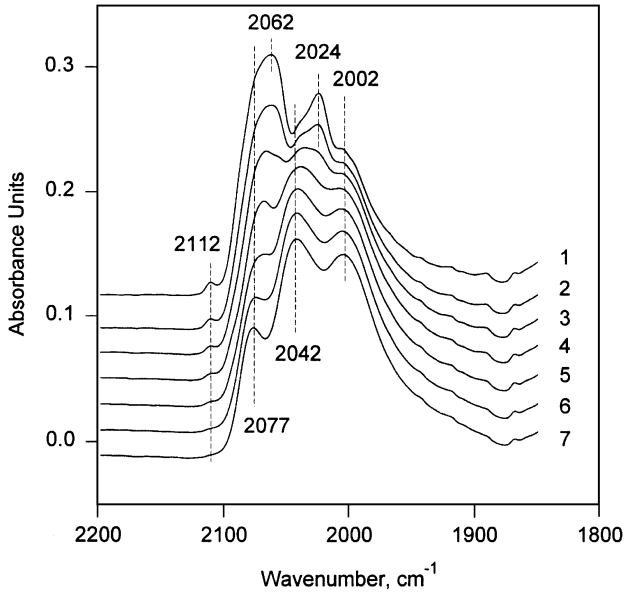

FIG. 3. Infrared spectra in the ν_{CO} region characterizing γ-Al_2O_3-supported $[Ir_4(CO)_{12}]$ after treatment in He under the following conditions: (1) 100°C; (2) 20 min at 100°C; (3) 40 min at 100°C; (4) 60 min at 100°C; (5) 80 min at 100°C; (6) 100 min at 100°C; (7) 120 min at 100°C.

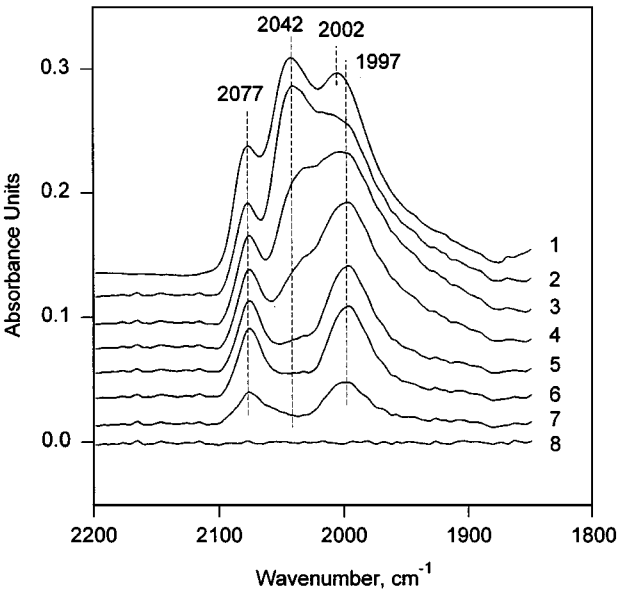

FIG. 4. Infrared spectra in the ν_{CO} region characterizing decarbonylation of γ-Al_2O_3-supported $[Ir_4(CO)_{12}]$ in He flow under the following conditions: (1) 120 min at 100°C; (2) 150°C; (3) 20 min at 150°C; (4) 40 min at 150°C; (5) 60 min at 150°C; (6) 120 min at 150°C; (7) 120 min at 220°C; (8) 300°C.

the spectrum recorded at 100°C than in that recorded at room temperature. The broad absorption band centered at 2029 cm^{-1} at 25°C (Fig. 1, spectrum 1) split into a strong band at 2024 cm^{-1} and a shoulder at 2042 cm^{-1} (Fig. 3, spectrum 1). The bands at 2112, 2077, 2062, 2042, 2024, and 2002 cm^{-1} match those of $[Ir_4(CO)_{12}]$ (13). Further changes in the infrared spectrum were observed over time as the temperature was held constant at 100°C for 2 h; the strong bands at 2062 and 2024 cm^{-1} disappeared, and the bands at 2077, 2042, and 2002 cm^{-1} became dominant (Fig. 3). These changes occurred without significant changes in the total absorption in the ν_{CO} region. An extraction of the surface species with THF at this point gave a solution with a spectrum virtually identical to that of $[Ir_4(CO)_{12}]$ in THF (Fig. 2, spectrum 2). Further increases in the treatment temperature led to decreased intensity of the ν_{CO} bands assigned to $[Ir_4(CO)_{12}]$, until finally, at 300°C, no ν_{CO} bands remained (Fig. 4).

Recarbonylation of γ-Al_2O_3-supported Ir_4 clusters. When the decarbonylated sample was treated with CO at room temperature, weak bands appeared in the ν_{CO} region, at 2076 and 2002 cm^{-1} (Fig. 5, spectrum 1). The positions of these bands were the same as those observed during the latter steps of decarbonylation of the original γ-Al_2O_3-supported $[Ir_4(CO)_{12}]$ sample (Fig. 4). Further treatment in flowing He as the temperature was ramped to 300°C led to the removal of these bands, with the behavior being similar to that observed during the removal of CO from the original supported $[Ir_4(CO)_{12}]$ (Fig. 5). When the sample

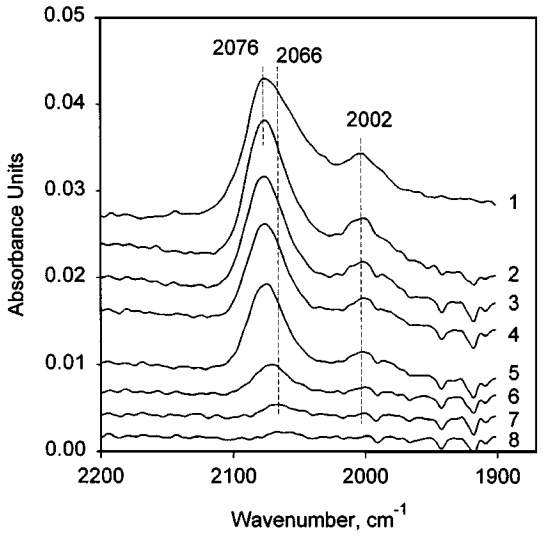

FIG. 5. Infrared spectra of CO adsorbed on sample prepared from $[Ir_4(CO)_{12}]$ on γ-Al_2O_3 and treated with He at 300°C, following treatment in He under the following conditions: (1) 25°C; (2) 70°C; (3) 220°C; (4) 260°C; (5) 300°C; (6) 20 min at 300°C; (7) 80 min at 300°C; (8) 100 min at 300°C.

was held in flowing CO at 150 or 200°C for 8 h, the resultant ν_{CO} spectrum included bands at 2112, 2072, 2029, and 2002 cm^{-1}, which are virtually identical to those characteristic of supported $[Ir_4(CO)_{12}]$ (Fig. 1).

Chemisorption of hydrogen on (partially) decarbonylated iridium clusters. Hydrogen chemisorption data characterizing γ-Al_2O_3-supported iridium clusters formed from $[Ir_4(CO)_{12}]$ after various treatments are summarized in Table 2. The data show that H/Ir values depend strongly on the degree of decarbonylation. The H/Ir value characterizing a completely decarbonylated sample (which had been treated in He at 300°C) was 0.13, in good agreement with previous observations for Ir_4/γ-Al_2O_3 prepared similarly

TABLE 2

Hydrogen Chemisorption on Supported Iridium Catalysts Formed from $[Ir_4(CO)_{12}]/\gamma$-Al_2O_3 by Treatment in He Flowing at Different Temperatures

Treatment gas	Temperature (°C)	Percentage of CO ligands left in supported iridium carbonyl cluster[a]	Chemisorption at 25°C, atomic ratio (H/Ir)
None	—	100	0.00
He	100	100	0.00
He	150	31.4	0.02
He	200	26.2	0.04
He	250	13.7	0.08
He	300	0.0	0.13
He	400	0.0	0.35

[a] Determined on the basis of infrared spectroscopy.

TABLE 3A

EXAFS Results at the Ir L_{III} Edge Characterizing the Species Formed by Adsorption of $[Ir_4(CO)_{12}]$ onto γ-Al_2O_3 from *n*-Pentane Solution at 25°C[a]

Shell	N	R (Å)	$10^3 \cdot \Delta\sigma^2$ (Å^2)	ΔE_0 (eV)	EXAFS reference
Ir–Ir	3.0 ± 0.1	2.66 ± 0.01	5.3 ± 0.1	1.0 ± 0.2	Pt–Pt
$Ir–O_{support}$	0.8 ± 0.1	2.29 ± 0.01	6.1 ± 0.6	2.0 ± 0.5	Pt–O
Ir–CO					
Ir–C	2.8 ± 0.1	1.86 ± 0.01	3.2 ± 0.1	5.8 ± 0.1	Ir–C
Ir–O*	3.1 ± 0.1	2.89 ± 0.01	1.8 ± 0.2	6.8 ± 0.1	Ir–O*

[a] Notation: N, coordination number; R, distance between absorber and backscatterer atoms; $\Delta\sigma^2$, Debye–Waller factor; ΔE_0, inner potential correction.

(14). A H/Ir value of 0.35 was found for the sample treated at 400°C. These H/Ir values characterizing the decarbonylated iridium clusters are markedly less than those typically observed for hydrogen chemisorption on supported iridium metal particles (15).

Details of EXAFS data analysis. The raw EXAFS data characterizing the samples treated under various conditions were analyzed according to the following procedure: The raw EXAFS data at the Ir L_{III} edge were first Fourier transformed with a k^3 weighting over the range $2.73 < k < 15.99$ Å^{-1} without any phase correction. The Fourier-transformed data were then inverse transformed in the range $0.1 < r < 4.40$ Å to isolate the main-shell contributions from low-frequency noise. With the difference file technique (11, 12), the Ir–Ir contributions in each sample, the largest in the EXAFS spectra, were first estimated and subsequently subtracted from the raw data. The difference file was expected to represent $Ir–O_{support}$ and Ir–CO* contributions. After optimizing the parameters for these two contributions, the first-guess Ir–Ir contributions were than added and compared with the raw data. The final parameters representing the high-Z (Ir–Ir) and low-Z (Ir–O and Ir–C) contributions were determined by multiple-shell fitting in r space and in k space with application of k^1 and

TABLE 3B

EXAFS Results at the Ir L_{III} Edge Characterizing the Species Formed by Decarbonylation of $[Ir_4(CO)_{12}]$ on γ-Al_2O_3 in He at 100°C[a]

Shell	N	R (Å)	$10^3 \cdot \Delta\sigma^2$ (Å^2)	ΔE_0 (eV)	EXAFS reference
Ir–Ir	3.0 ± 0.1	2.66 ± 0.01	5.3 ± 0.1	1.0 ± 0.3	Pt–Pt
$Ir–O_{support}$	0.8 ± 0.1	2.29 ± 0.01	6.1 ± 0.9	2.0 ± 0.8	Pt–O
Ir–CO					
Ir–C	3.0 ± 0.1	1.85 ± 0.01	5.4 ± 0.2	6.9 ± 0.5	Ir–C
Ir–O*	2.9 ± 0.1	2.88 ± 0.01	1.0 ± 0.1	7.5 ± 0.1	Ir–O*

[a] Notation as in Table 3A.

TABLE 3C

EXAFS Results at the Ir L_{III} Edge Characterizing the Species Formed by Decarbonylation of $[Ir_4(CO)_{12}]$ on γ-Al_2O_3 in He at 200°C[a]

Shell	N	R (Å)	$10^3 \cdot \Delta\sigma^2$ (Å^2)	ΔE_0 (eV)	EXAFS reference
Ir–Ir	3.0 ± 0.01	2.68 ± 0.01	5.6 ± 0.2	6.4 ± 0.3	Pt–Pt
Ir–$O_{support}$					
Ir–O_s	0.7 ± 0.1	2.18 ± 0.01	0.8 ± 0.5	-8.0 ± 1.2	Pt–O
Ir–O_l	1.4 ± 0.2	2.70 ± 0.01	10.0 ± 1.2	-0.7 ± 0.7	Pt–O
Ir–CO					
Ir–C	0.7 ± 0.1	1.84 ± 0.01	-0.4 ± 0.3	-7.0 ± 1.3	Ir–C
Ir–O*	0.7 ± 0.1	2.89 ± 0.01	3.0 ± 0.9	0.0 ± 0.20	Ir–O*

[a] Notation as in Table 3A; the subscripts s and l refer to short and long, respectively.

k^3 weighting (16, 17) over the ranges $3.6 < k < 15$ Å^{-1} and $0.1 < r < 4.0$ Å. The maximum number of free parameters used to fit the main-shell contributions was 20. The statistically justified number of free parameters (n), estimated from the Nyquist theorem (16), $n = (2\Delta k \Delta r/\pi) + 1$, where Δk and Δr are the k and r ranges used to fit data, was approximately 29.

The parameters determined by this fitting routine are summarized in Tables 3 and 4, and comparisons of the data and fits in r space are shown in Figs. 6 and 7. The residual spectra determined by subtracting the Ir–Ir + Ir–$O_{support}$ contributions from the raw EXAFS data, giving evidence of Ir–CO interactions, are shown in Figs. 6D and 6E. The XDAP software (10) was used to obtain rough estimates of the error bounds in the EXAFS parameters, as shown in Tables 3 and 4. These error bounds represent precisions (reproducibilities) determined from statistical analysis of the data, not accuracies.

Toluene hydrogenation catalysis. The catalytic results characterizing the γ-Al_2O_3-supported iridium clusters decarbonylated to various degrees are summarized in Table 5. After the initial break-in period of about 30 min, when a decrease in activity was observed, each catalyst was stable for at least 6 h onstream. The reaction rates reported here correspond to 2 h onstream, which is represented as steady-state operation. Calculations with standard methods showed that the reaction was slow enough that the influence of transport phenomena on the rate was negligible.

The reported turnover frequencies (Table 5), which are defined unconventionally, were calculated by normalizing the reaction rates with respect to the fraction of iridium atoms free of CO ligands and thus available to facilitate catalysis; the fraction of available iridium atoms was estimated from the infrared band intensities, with the value being zero for $[Ir_4(CO)_{12}]$ and one for the fully decarbonylated clusters. The reaction rate per total Ir atom increased as the first CO ligands were removed from the catalyst, approaching a nearly constant value when about 70% of the CO ligands had been removed (Fig. 8, Table 5). The turnover frequency was roughly constant for all the (partially) decarbonylated catalysts (Table 5).

The apparent activation energies determined from the temperature dependence of the reaction rates for the variously decarbonylated catalyst were found to be in the range 10–13 kcal/mol, which is typical for supported iridium catalysts for this reaction (3).

TABLE 3D

EXAFS Results at the Ir L_{III} Edge Characterizing the Species Formed by Decarbonylation of $[Ir_4(CO)_{12}]$ on γ-Al_2O_3 in He at 300°C[a]

Shell	N	R (Å)	$10^3 \cdot \Delta\sigma^2$ (Å^2)	ΔE_0 (eV)	EXAFS reference
Ir–Ir	3.0 ± 0.1	2.67 ± 0.01	5.0 ± 0.2	-3.0 ± 0.3	Pt–Pt
Ir–$O_{support}$					
Ir–O_s	0.7 ± 0.1	2.21 ± 0.01	1.3 ± 0.4	-10.1 ± 0.5	Pt–O
Ir–O_l	1.3 ± 0.1	2.67 ± 0.01	0.4 ± 0.4	-2.0 ± 0.3	Pt–O
Ir–Al	0.1 ± 0.1	1.73 ± 0.02	1.4 ± 0.7	5.5 ± 5.2	Ir–Al

[a] Notation as in Table 3C.

TABLE 3E

EXAFS Results at the Ir L_{III} Edge Characterizing the Species Formed by Decarbonylation of $[Ir_4(CO)_{12}]$ on γ-Al_2O_3 in He at 400°C[a]

Shell	N	R (Å)	$10^3 \cdot \Delta\sigma^2$ (Å^2)	ΔE_0 (eV)	EXAFS reference
Ir–Ir	5.2 ± 0.1	2.67 ± 0.01	5.0 ± 0.1	-5.0 ± 0.1	Pt–Pt
Ir–$O_{support}$					
Ir–O_s	0.8 ± 0.1	2.17 ± 0.01	8.1 ± 0.8	-8.0 ± 1.0	Pt–O
Ir–O_l	0.9 ± 0.1	2.63 ± 0.01	-1.7 ± 0.4	3.9 ± 0.3	Pt–O
Ir–Al	0.1 ± 0.1	1.77 ± 0.01	-2.8 ± 0.7	-1.4 ± 4.2	Ir–Al

[a] Notation as in Table 3C.

TABLE 4

EXAFS Results at the Ir L_{III} Edge Characterizing the Iridium Clusters Formed by CO Treatment at 200°C for 8 h of Sample That Had Previously Been Decarbonylated in He at 300°C[a]

Shell	N	R (Å)	$10^3 \cdot \Delta\sigma^2$ (Å^2)	ΔE_0 (eV)	EXAFS reference
Ir–Ir	3.0 ± 0.1	2.70 ± 0.01	2.8 ± 0.1	2.4 ± 0.1	Pt–Pt
Ir–$O_{support}$	0.6 ± 0.1	2.22 ± 0.01	0.6 ± 0.1	-12.5 ± 0.1	Pt–O
Ir–CO					
Ir–C	2.1 ± 0.1	1.85 ± 0.01	8.2 ± 0.1	-6.2 ± 0.1	Ir–C
Ir–O*	2.8 ± 0.1	2.86 ± 0.01	4.2 ± 0.1	5.9 ± 0.1	Ir–O*

[a] Notation as in Table 3C.

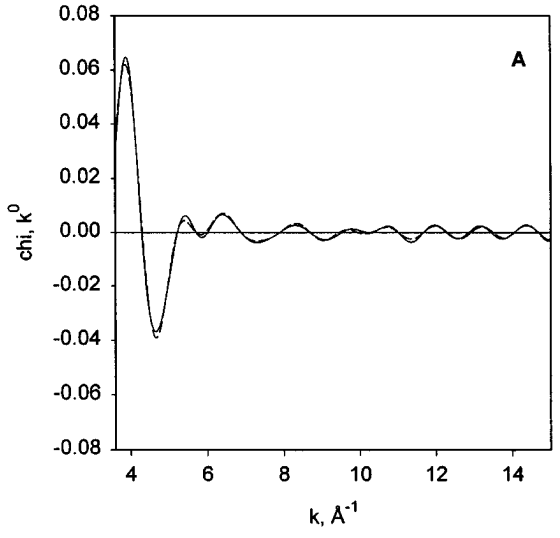
A
chi, k0
k, Å-1

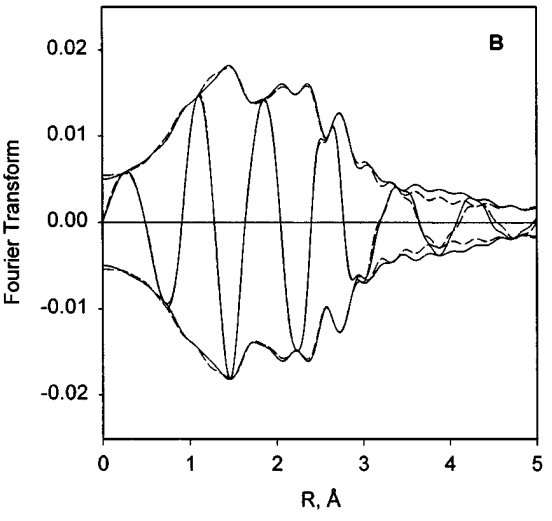
B
Fourier Transform
R, Å

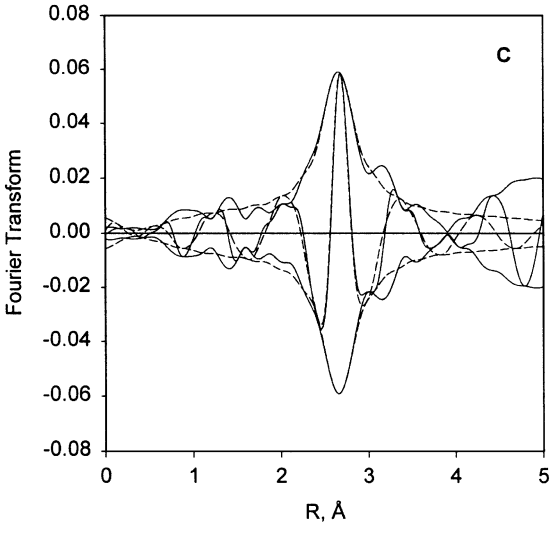
C
Fourier Transform
R, Å

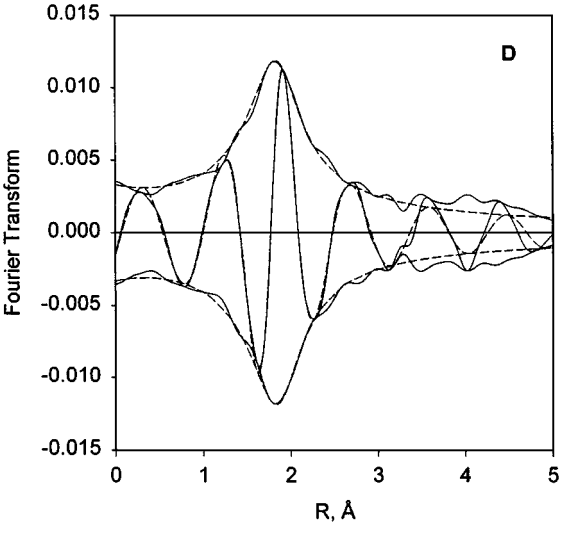
D
Fourier Transform
R, Å

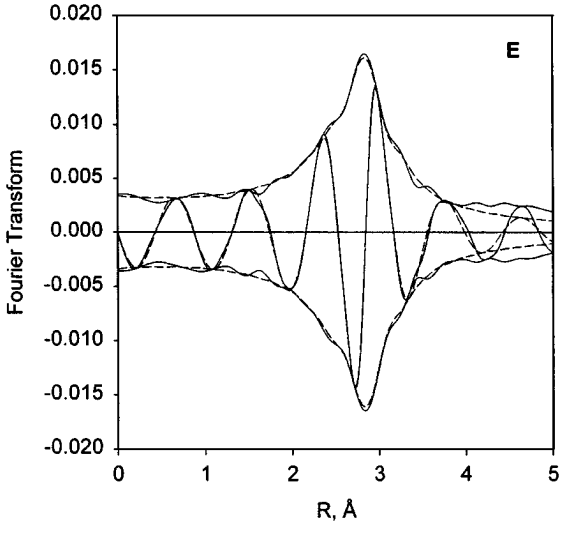
E
Fourier Transform
R, Å

TABLE 5

Toluene Hydrogenation Catalyzed by Al_2O_3-Supported Iridium Clusters

Temperature of treatment in He (°C)	Approximate percentage of CO ligands removed from supported iridium carbonyl cluster[a]	Catalytic activity[b] (mmol MCH/mol Ir · s)	TOF × 10^3 [c] (s^{-1})
No treatment	0.0	0.0	—
100	0.0	0.2	—
150	68.6	7.7	11.2
200	73.8	10.9	14.8
250	86.3	11.1	12.9
300	100	10.9	10.9
400	100	14.5	—

[a] Determined from infrared data.

[b] Reaction at 60°C, $P_{toluene} = 50$ Torr, and $P_{hydrogen} = 710$ Torr.

[c] Turnover frequency represented here as reaction rate normalized by fraction of iridium atoms without CO ligands available for H_2 and toluene adsorption; no account was taken of the possibility that some of the iridium atoms would be inaccessible because of blockage by the support.

DISCUSSION

Formation of $[Ir_4(CO)_{12}]$ on γ-Al_2O_3

Interactions between iridium carbonyls and the surfaces of basic metal oxides typically involve reactions of support surface OH groups with the iridium carbonyls, leading to the formation of supported iridium carbonylate anions (4, 5, 18). The formation of such anions manifests itself by the shifting of terminal ν_{CO} bands to lower frequencies (19). The reactions of $[Ir_4(CO)_{12}]$ with the surfaces of basic metal oxides are analogous to the reactions of $[Ir_4(CO)_{12}]$ and other iridium carbonyls in basic solutions (20, 21). In contrast, however, relatively little is known about the interactions between iridium carbonyls and the surfaces of neutral or acidic supports.

The infrared spectra of the samples formed by slurrying $[Ir_4(CO)_{12}]$ with γ-Al_2O_3 powder were found to be virtually the same as those reported for crystalline $[Ir_4(CO)_{12}]$ (13, 22). The result that almost the same band positions in the ν_{CO} region were observed for $[Ir_4(CO)_{12}]$ before and after interaction with γ-Al_2O_3 indicates that the iridium clusters did not decompose during adsorption and did not form iridium cluster anions. Rather, supported $[Ir_4(CO)_{12}]$ simply formed. Because $[Ir_4(CO)_{12}]$ could be recovered from the γ-Al_2O_3 surface by simple extraction with THF at 25°C (Fig. 2, spectrum 1), we infer that the clusters were only weakly adsorbed on the surface. These results are similar to those reported for $[Ir_4(CO)_{12}]$ supported on SiO_2 (23).

The EXAFS data provide additional information about the structure of the surface species. The crystallographic parameters reported for crystalline $[Ir_4(CO)_{12}]$ (24) are consistent with the suggestion that the four iridium atoms are arranged in a regular tetrahedron, with each bonded to three other iridium atoms (at a distance of 2.69 Å) and to three terminal CO ligands (with Ir–C and Ir–O* distances of 1.87 and 3.01 Å, respectively). The Ir L_{III} edge EXAFS results characterizing the sample formed by the adsorption of $[Ir_4(CO)_{12}]$ on γ-Al_2O_3 indicate an average first-shell Ir–Ir coordination number of 3.0 and an average Ir–Ir distance of 2.66 Å (Table 3A), as well as an average Ir–C coordination number of 2.8 with an average Ir–C bond distance of 1.86 Å. Furthermore, a second-shell Ir–O* contribution with an average coordination number of 3.1 and a distance of 2.89 Å was observed, signifying the contribution from the oxygen atoms of the carbonyl ligands. Thus, the observed first-shell Ir–Ir coordination number is the same within experimental error as that determined for crystalline $[Ir_4(CO)_{12}]$ (24), indicating that the iridium clusters were adsorbed intact on γ-Al_2O_3 and that the tetrahedral Ir–Ir cluster frame was retained. However, the Ir–Ir and Ir–O* distances are somewhat less than the respective values observed for crystalline $[Ir_4(CO)_{12}]$ (24). These differences suggest that distortion of the cluster took place as a result of interaction with the γ-Al_2O_3 surface, but it was not sufficient to disrupt the metal frame.

Together with Ir–Ir and Ir–CO contributions, $Ir–O_{support}$ contributions were observed. The $Ir–O_{support}$ contributions, with an average Ir–O distance of 2.29 Å and an average coordination number of about 0.8, are typical of noble metals supported on metal oxides (25) and indicate the interactions of iridium atoms with surface oxygen atoms of γ-Al_2O_3. If, during adsorption, oxidation of the iridium had occurred, we would expect Ir–O contributions at a shorter (bonding) distance of about 1.95 Å, similar to what has been observed for totally oxidized Ir/γ-Al_2O_3 samples (26).

In summary, the infrared and EXAFS data indicate that $[Ir_4(CO)_{12}]$ was adsorbed intact on partially

FIG. 6. Results of analysis of Ir L_{III} edge EXAFS data obtained with the best calculated coordination parameters characterizing the γ-Al_2O_3-supported $[Ir_4(CO)_{12}]$. (A) Experimental EXAFS function (solid line) and sum of the calculated Ir–Ir + Ir–$O_{support}$ + Ir–C + Ir–O* contributions (dashed line). (B) Imaginary part and magnitude of uncorrected Fourier transform (k^0 weighted) of experimental EXAFS (solid line) and sum of the calculated Ir–Ir + Ir–$O_{support}$ + Ir–C + Ir–O* contributions (dashed line). (C) Imaginary part and magnitude of phase- and amplitude-corrected Fourier transform (k^0 weighted) of raw data minus the calculated Ir–$O_{support}$ + Ir–C + Ir–O* contributions (solid line) and calculated Ir–Ir contributions (dashed line). (D) Residual spectrum illustrating Ir–C contributions of carbonyl ligands: imaginary part and magnitude of phase-corrected Fourier transform (k^0 weighted) of raw data minus the calculated Ir–Ir + Ir–$O_{support}$ + Ir–O* contributions (solid line) and calculated Ir–C contributions (dashed line). (E) Residual spectrum illustrating Ir–O* contributions of carbonyl ligands: imaginary part and magnitude of phase-corrected Fourier transform (k^0 weighted) of raw data minus the calculated Ir–Ir + Ir–$O_{support}$ + Ir–C contributions (solid line) and calculated Ir–O* contributions (dashed line).

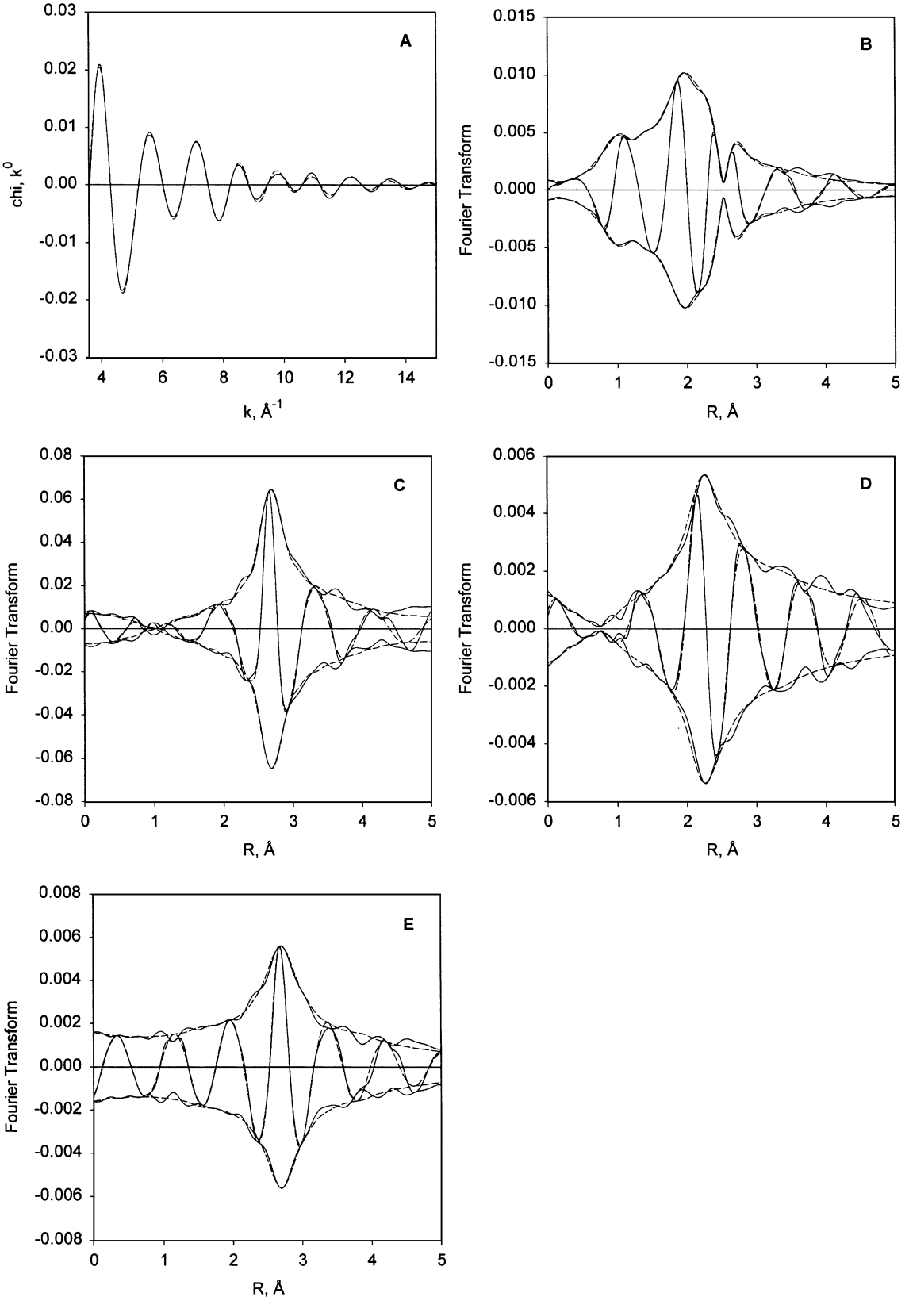
A
chi, k0
k, Å-1
B
Fourier Transform
R, Å
C
Fourier Transform
R, Å
D
Fourier Transform
R, Å
E
Fourier Transform
R, Å

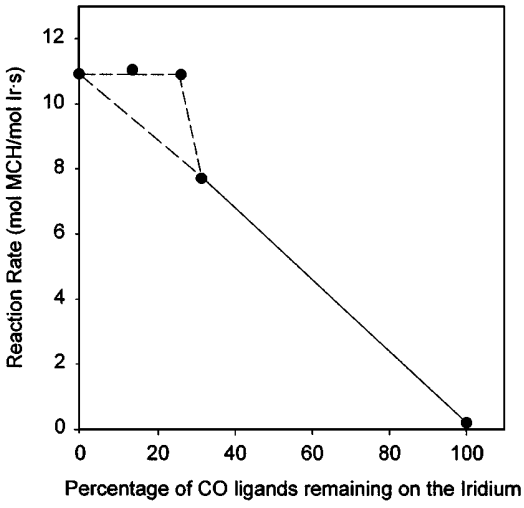

FIG. 8. Toluene hydrogenation catalyzed by partially decarbonylated $[Ir_4(CO)_{12}]$ clusters supported on γ-Al_2O_3: dependence of the reaction rate on the degree of decarbonylation of the supported clusters.

dehydroxylated γ-Al_2O_3. The interactions of the iridium carbonyl clusters with the γ-Al_2O_3 surface were weak enough to allow reversible distortion of the ligand sphere of the cluster without substantial loss of CO ligands and without disruption of the tetrahedral cluster frame.

Infrared and EXAFS Evidence of Formation of Partially Decarbonylated Tetrairidium Clusters on γ-Al_2O_3

Decarbonylation of the supported $[Ir_4(CO)_{12}]$ was carried out with the sample in flowing He as the temperature was ramped at 3°C/min from 25 to 300°C. The ν_{CO} infrared spectrum shows that the supported $[Ir_4(CO)_{12}]$ remained nearly intact at 100°C. As the temperature was held constant with the sample in flowing He at 100°C, changes occurred in the infrared spectra (Fig. 3), with the bands at 2062 and 2024 cm^{-1} disappearing and the ν_{CO} bands at 2077, 2042, and 2002 cm^{-1} becoming dominant. These band positions match some of the ν_{CO} bands in crystalline $[Ir_4(CO)_{12}]$ (13). We regard it as important that the total absorption in the ν_{CO} region (the area under the CO bands) remained nearly constant during this transformation. Since total absorbance in the ν_{CO} region is expected to be approximately proportional to the number of surface CO ligands, we infer that changes observed in the infrared spectra with increasing temperatures of He treatment up to 100°C indicate changes in the interactions between the iridium clusters and the support and not decarbonylation. Consequently, we infer that the structure of the supported $[Ir_4(CO)_{12}]$ clusters changed, but the data are not sufficient to determine how.

Furthermore, the result that $[Ir_4(CO)_{12}]$ was recovered intact from the γ-Al_2O_3 surface as a result of extraction with THF (Fig. 2, spectrum 2) is consistent with the inference that $[Ir_4(CO)_{12}]$ remained intact on the γ-Al_2O_3 surface prior to the extraction.

The Ir L_{III} edge EXAFS data provide additional evidence supporting the conclusion that the cluster frame remained intact on heating in He. After He treatment of $[Ir_4(CO)_{12}]/\gamma$-Al_2O_3 at 100°C, the average Ir–Ir coordination number was 3.0, with an average Ir–Ir distance of 2.66 Å (Table 3B), agreeing closely with the values for crystalline $[Ir_4(CO)_{12}]$. The Ir–CO contributions associated with CO ligands were also observed, with average Ir–C and Ir–O* distances of 1.85 and 2.88 Å, respectively (Table 3B). Thus, the EXAFS data characterizing the supported clusters treated at 100°C (Table 3B) were found to be the same, within experimental error, as those determined for the original sample made by adsorption of $[Ir_4(CO)_{12}]$ on γ-Al_2O_3 (Table 3A). These data are in agreement with the infrared and extraction data, indicating that supported $[Ir_4(CO)_{12}]$ was stable in flowing He under the low-temperature ($\leq$100°C) treatment conditions.

According to the infrared data, the intensity of each of the peaks in the ν_{CO} region decreased when the temperature of He treatment was increased beyond 100°C. The band at 2042 cm^{-1} decreased in intensity as the temperature increased and was the first to disappear, leaving two bands of approximately equal intensity at 2077 and 1997 cm^{-1} (Fig. 4). The intensities of these bands decreased with increasing treatment temperature, and they disappeared when the temperature reached 300°C, indicating that the sample was fully decarbonylated. The bands at 2077 and 1997 cm^{-1} observed during the last phase of decarbonylation are similar to those attributed to $Ir(CO)_2$ species (2070 and 2000 cm^{-1}) formed from $[Ir(CO)_2(acac)]$ on γ-Al_2O_3 (22) and to the ν_{CO} spectrum (2082 and 2000 cm^{-1}) observed after treatment of $[Ir_4(CO)_{12}]$/NaY zeolite in oxygen and the ensuing oxidative fragmentation (27). The

FIG. 7. Results of analysis of Ir L_{III} edge EXAFS data obtained with the best calculated coordination parameters characterizing supported iridium clusters formed by the decarbonylation of γ-Al_2O_3-supported $[Ir_4(CO)_{12}]$ in flowing He at 300°C: (A) Experimental EXAFS function (solid line) and sum of the calculated Ir–Ir + Ir–$O_{support}$ (Ir–O_s and Ir–O_l) + Ir–Al contributions (dashed line). (B) Imaginary part and magnitude of uncorrected Fourier transform (k^0 weighted) of experimental EXAFS (solid line) and sum of the calculated Ir–Ir + Ir–$O_{support}$ (Ir–O_s and Ir–O_l) + Ir–Al contributions (dashed line). (C) Imaginary part and magnitude of phase- and amplitude-corrected Fourier transform (k^0 weighted) of raw data minus the calculated Ir–$O_{support}$ (Ir–O_s and Ir–O_l) + Ir–Al contributions (solid line) and calculated Ir–Ir contributions (dashed line). (D) Residual spectrum illustrating Ir–$O_{support}$ (Ir–O_s) contributions: imaginary part and magnitude of phase-corrected Fourier transform (k^0 weighted) of raw data minus the calculated Ir–Ir + Ir–$O_{support}$ (Ir–O_l) contributions (solid line) and calculated Ir–O_s contributions (dashed line). (E) Residual spectrum illustrating Ir–$O_{support}$ (Ir–O_l) contributions: imaginary part and magnitude of phase-corrected Fourier transform (k^0 weighted) of raw data minus the calculated Ir–Ir + Ir–$O_{support}$ (Ir–O_s) + Ir–Al contributions (solid line) and calculated Ir–O_l contributions (dashed line).

observed decarbonylation profile is similar to that observed during decarbonylation of $[Ir_4(CO)_{12}]/\gamma\text{-}Al_2O_3$ under vacuum (28). It was suggested that the appearance of a pair of bands, at 2072 and 1995 cm^{-1}, indicates that oxidative fragmentation of $[Ir_4(CO)_{12}]$ occurred during decarbonylation under vacuum, leading to the formation of a $Ir^+(CO)_2$ surface species (28). However, the EXAFS data at the Ir L_{III} edge obtained for the samples formed from $[Ir_4(CO)_{12}]/\gamma\text{-}Al_2O_3$ that had been decarbonylated at different temperatures (Tables 3B–3D) indicate that only Ir–Ir first-shell contributions with an average Ir–Ir coordination number of 3.0 and an average Ir–Ir distance of about 2.67 Å were observed at different treatment temperatures. The absence of Ir–Ir contributions at distances greater than the first-shell Ir–Ir coordination distance is consistent with the suggestion that clusters larger than Ir_4 were not formed and that the nuclearity of the iridium carbonyl precursor was retained.

In agreement with the infrared data, the EXAFS data indicate that the Ir–CO contributions decreased with an increase in decarbonylation temperature, accompanied by an increase in the intensities of the $Ir\text{–}O_{support}$ contributions. Evidently, as the bulky CO ligands were removed, there was greater contact between the metal cluster frame and the support. The trend in the data shows that the shorter $Ir\text{–}O_{support}$ distance decreased as the degree of decarbonylation increased. This distance, 2.19 ± 0.02 Å for the samples treated at temperatures of 200°C and higher, is a chemical bonding distance characteristic of cationic iridium and oxygen in various organic ligands (29); this result suggests that the iridium bears a positive charge.

In addition, longer Ir–O contributions were observed, with an average Ir–O coordination number of about 1.3 at an average distance of 2.7 Å (Tables 3C and 3D). Similarly, such long metal–oxygen contributions have been observed for iridium (30) and other noble metals (25) on various metal oxide and zeolite supports. The nature of these relatively long metal–oxygen contributions is still a matter of discussion; they may be explained, for example, by the interaction of supported iridium atoms with surface hydroxyl groups located at the metal–support interface (31), but they are too long to be explained as Ir–O bonds. The present results show that the increased metal–support interactions resulting from cluster decarbonylation did not lead to oxidative fragmentation of the tetrahedral Ir_4 frame, as had been suggested by Tanaka *et al*. (28) on the basis of infrared spectroscopy alone. We might expect that if the suggested $Ir^+(CO)_2$ species were formed on the surface as a result of oxidative fragmentation, only the $Ir\text{–}O_{support}$ and Ir–CO contributions would have been observed in the EXAFS spectra, with no evidence of Ir–Ir contributions, contrary to the observations. Thus, on the basis of the EXAFS data, we might infer that the pair of bands observed in the infrared spectra at 2077 and 1997 cm^{-1} during decarbonylation in He at temperatures higher than 100°C should be attributed to iridium carbonyl clusters having an average of only two CO ligands per iridium atom, with each of these ligands connected to each iridium atom in the Ir_4 tetrahedron. However, the possibility of partial iridium oxidation (or perhaps electron withdrawal from iridium atoms) remains—possibly resulting from interactions of iridium with oxygen atoms at the support surface.

In contrast to our results, however, Tanaka *et al*. (28), working with a sample made from $[Ir_4(CO)_{12}]$ on uncalcined $\gamma\text{-}Al_2O_3$ that had been treated in a similar way, observed infrared spectra indicating oxidative fragmentation of the $[Ir_4(CO)_{12}]$ in flowing He starting at 75°C (28). And Kawi *et al*. (22), working with a sample formed by carbonylation of a sample made by adsorption of $[Ir(CO)_2(acac)]$ on $\gamma\text{-}Al_2O_3$, observed decreasing infrared absorption in the ν_{CO} region without evidence of oxidative fragmentation as the sample was treated in flowing He; the spectra were interpreted as evidence of the formation of $[HIr_4(CO)_{11}]^-$ on the support surface, which was attributed to a nucleophilic attack of surface hydroxyl groups on the CO ligands of $[Ir_4(CO)_{12}]$, with the chemistry being similar to that observed in the reaction of $[Ir_4(CO)_{12}]$ with the partially hydroxylated MgO surface (19). The results of Tanaka *et al*. and Kawi *et al*. are different from those reported here. We suggest that the surface chemistry was different in the different samples, at least in part because of differences in the degree of surface hydroxylation or hydration and the sensitivity of the surface chemistry to the density of hydroxyl groups or water (32); this suggestion is in need of testing.

Recarbonylation of γ-Al_2O_3-Supported Ir_4 Clusters

After complete decarbonylation of the $\gamma\text{-}Al_2O_3$-supported $[Ir_4(CO)_{12}]$ clusters, the sample was cooled to room temperature and treated with CO. The infrared spectra show low-intensity bands in the ν_{CO} region, at 2076 and 2002 cm^{-1} (Fig. 5). The positions of these bands in the recarbonylated sample are the same as those observed during decarbonylation of the original $\gamma\text{-}Al_2O_3$-supported $[Ir_4(CO)_{12}]$ at higher temperatures. Furthermore, the behavior of these bands during heating of the sample in He was similar to that observed for CO chemisorbed on metal particles (33). With increasing treatment temperature, the band at 2002 cm^{-1} disappeared first, and the band at 2076 cm^{-1} shifted by 10 cm^{-1} to a lower frequency. This change might be explained by the decreasing dipole–dipole coupling between adsorbed CO ligands with decreasing surface coverage (34). Comparable to the ν_{CO} bands in the spectrum of $[Ir_4(CO)_{12}]$, the observed ν_{CO} bands were removed from the spectrum of the supported iridium clusters after treatment in He at 300°C. Thus, the infrared data show that after the treatment of the decarbonylated Ir_4 clusters with CO at room temperature, partially carbonylated tetrairidium clusters were formed, but the regeneration of

the original $[Ir_4(CO)_{12}]$ clusters did not take place. Similarly, decarbonylation of $[Ir_4(CO)_{12}]$ on MgO followed by recarbonylation has been observed to give iridium carbonyls other than the original $[HIr_4(CO)_{11}]^-$ (35).

Prolonged treatment of decarbonylated γ-Al_2O_3-supported Ir_4 clusters with CO at 150 or 200°C led to approximately 70 and 90% restoration of the CO absorbance, respectively. The observed infrared spectrum was very similar to that of the original γ-Al_2O_3-supported $[Ir_4(CO)_{12}]$ (Fig. 1). The ν_{CO} bands observed at 2112, 2072, 2029, and 2002 cm^{-1} after the recarbonylation at 150–200°C are virtually the same as the major infrared bands characteristic of $[Ir_4(CO)_{12}]$ (13). However, a precise comparison of infrared spectra characterizing the original supported $[Ir_4(CO)_{12}]$ with those of recarbonylated Ir_4 clusters shows that the band at 2062 cm^{-1} observed in the spectrum of the original supported $[Ir_4(CO)_{12}]$ was not observed after recarbonylation, and the intensity of the band at 2029 cm^{-1} was less than that of the original sample (Fig. 1). This comparison shows that the $[Ir_4(CO)_{12}]$ clusters were only partially reconstructed on the γ-Al_2O_3 surface during treatment with CO at 150–200°C.

The EXAFS data confirm this conclusion. After treatment of decarbonylated Ir_4 clusters with CO at 200°C, the first-shell Ir–Ir coordination number was found to be 3.0 (Table 4) at a distance of 2.7 Å. These data are consistent with the suggestion that supported iridium clusters retained the nuclearity of the $[Ir_4(CO)_{12}]$ precursor, not only during impregnation and decarbonylation, but during the recarbonylation as well. The Ir–Ir distance of 2.70 Å observed after recarbonylation is greater than that (2.67 Å) observed after adsorption of $[Ir_4(CO)_{12}]$ on γ-Al_2O_3 and greater than that characteristic of the (partially) decarbonylated supported clusters. However, the difference is about the same as the likely uncertainty in the data, approximately ±1% for the Ir–Ir distance. If the difference is more than an indication of experimental error, it implies that CO interacts with iridium atoms as an electron donor ligand. Since the Ir–C and Ir–O* coordination numbers observed in recarbonylated sample (Table 4) are somewhat different from those observed after adsorption of $[Ir_4(CO)_{12}]$ on γ-Al_2O_3, we infer that the stoichiometric CO/Ir ratio in the recarbonylated Ir_4 clusters could be different from that observed for the $[Ir_4(CO)_{12}]$ precursor.

In summary, the infrared and EXAFS data reported here provide the first evidence of the possibility of reconstruction of iridium carbonyl clusters from decarbonylated precursors on an amorphous support surface. The tetrairidium frame was maintained intact during the decarbonylation/recarbonylation process.

In contrast to the results reported here, increases in metal–metal coordination numbers have been observed for highly dispersed supported metals, including Pd (36, 37), Pt (38), and Ir (22); these results indicate that metal aggregation accompanied CO adsorption. The (exceptional) recarbonylation of Ir_4 clusters without changes in cluster nuclearity, as observed in the work reported here, is comparable to what has been demonstrated by infrared spectroscopy for iridium clusters that had been decarbonylated in the supercages of NaY zeolite (27).

Hydrogen Chemisorption on Supported Iridium Clusters

$[Ir_4(CO)_{12}]/\gamma$-Al_2O_3 was decarbonylated in He at various temperatures to give a family of partially decarbonylated tetrairidium clusters on γ-Al_2O_3 to allow measurements of the effects of the remaining CO ligands on hydrogen chemisorption and catalytic performance. The results are summarized in Table 2. As stated above, the EXAFS and infrared results indicate that the γ-Al_2O_3-supported $[Ir_4(CO)_{12}]$ was structurally indistinguishable from the clusters in the sample treated under helium at 100°C. No hydrogen chemisorption was observed on these samples (Table 2), in agreement with expectation that coordinatively unsaturated iridium atoms are required for hydrogen chemisorption—the surface iridium atoms were not available to hydrogen because of the presence of the carbonyl ligands.

Increases in the treatment temperature led to increases in the hydrogen chemisorption as the tetrairidium clusters were systematically decarbonylated (Table 2). The highest H/Ir value of about 0.13 was observed for the sample treated in He at 300°C. This sample was judged on the basis of infrared and EXAFS data to be fully decarbonylated. The observed H/Ir ratio is essentially the same as those reported for Ir_4/γ-Al_2O_3 (14) and Ir_4/MgO (35) samples prepared by adsorption of $[Ir_4(CO)_{12}]$ followed by decarbonylation; these samples are represented as supported Ir_4 clusters on the basis of EXAFS spectroscopy.

Typically, the ratio of hydrogen atoms to surface metal atoms characteristic of supported noble metals approaches unity as the particle size becomes smaller, but in some cases values even larger than one have been observed (15). However, the hydrogen chemisorption data reported here, together with those observed for other supported Ir_4 samples (14, 35), are consistent with the results reported by Kubo *et al.* (39), who observed values of H/Pt less than 1 for highly dispersed Pt/NaY zeolite samples.

It is still not evident why small iridium clusters chemisorb less hydrogen than larger iridium clusters or bulk iridium. The results are consistent with the suggestion that iridium dispersed on the surface in small clusters might lack the character of bulk metallic iridium; we regard the clusters as quasi-molecular and the support as a multidentate ligand (3); the EXAFS evidence of the metal–support interface is consistent with this suggestion (40).

The EXAFS (Table 3E) and chemisorption data (Table 2) show that as the temperature of treatment of the supported clusters in He increased to 400°C, the Ir–Ir

first-shell coordination number increased (to 5.2) and the H/Ir value increased (to 0.35). Thus, these data clearly show that even small changes in the iridium cluster size lead to substantial changes in the H/Ir ratio determined by chemisorption. Since there is a strong correlation between hydrogen chemisorption and the Ir–Ir coordination number, we conclude that the attainable surface coverage of iridium by hydrogen can be controlled by variation of the iridium cluster size; thus, the chemisorption data are consistent with the observation that the catalytic properties are dependent on the cluster size, even for structure-insensitive reactions (3, 14).

Catalytic Properties of Supported Tetrairidium Clusters

EXAFS experiments carried out with similarly prepared catalysts used under the same conditions showed that the nuclearity of the γ-Al_2O_3-supported clusters did not change (within experimental error) during catalysis (3).

The toluene hydrogenation reaction is regarded as structure insensitive, taking place with roughly the same turnover frequencies on the surfaces of metal particles of different sizes (41). According to Lin and Vannice (42), the mechanism of this reaction on particles of supported platinum involves dissociative chemisorption of H_2 on the metal surface with subsequent insertion of hydrogen atoms in the aromatic ring of adsorbed toluene. Our experimentally determined apparent activation energies for the decarbonylated and partially decarbonylated supported iridium clusters are in the range 10–13 kcal/mol, in good agreement with values typically observed for supported iridium and platinum catalysts (3, 43). This comparison may indicate that the mechanism of toluene hydrogenation on supported iridium clusters is similar to that inferred by Lin and Vannice (42) for the reaction on platinum particles. Under typical conditions of toluene hydrogenation, the first insertion of hydrogen is the rate-determining step (42). However, when the concentration of hydrogen on the surface of a metal is limited, as is expected for Ir_4/γ-Al_2O_3 (on the basis of the chemisorption data), it is expected that this rate-determining step (and possibly other steps involving adsorbed hydrogen and toluene) in the formation of methylcyclohexane may be slowed down relative to the rates of the reaction on iridium metal.

The toluene hydrogenation activity of the original $[Ir_4(CO)_{12}]/\gamma$-Al_2O_3 and that of the sample that had been treated in He at only 100°C were very small. As these samples were held in the flow reactor, the activity increased, presumably because some decarbonylation occurred with the samples in H_2. We infer that $[Ir_4(CO)_{12}]$ itself on the support was catalytically inactive, which is expected, because $[Ir_4(CO)_{12}]$ is coordinatively saturated with CO ligands.

As the temperature of treatment of the supported iridium carbonyl clusters increased, the degree of decarbonylation increased, and the catalytic reaction rate (expressed as moles of methylcyclohexane formed/mole of Ir · second) also increased (Fig. 8). The data are consistent with the suggestion that only metal sites accessible for toluene and hydrogen adsorption facilitate the reaction.

The data indicate an approximate equality of the (unconventionally defined) turnover frequencies of the (partially) decarbonylated catalysts. This result shows that the catalytic activity of the exposed iridium atoms is only weakly affected by the carbonyl ligands, once the clusters have become coordinatively unsaturated. Evidently, the ligand effect is small, but we emphasize that the data do not allow a separation of the effects of the CO and support ligands.

The catalytic activities of the three samples (per total Ir atom) with more than about 70% of the CO removed were all nearly the same (Table 5, Fig. 8). It is not evident why the catalytic reaction rate is nearly insensitive to the degree of decarbonylation exceeding about 70%. We might speculate that each Ir_4 cluster constitutes a single catalytic site and that removal of the first CO ligands from $[Ir_4(CO)_{12}]$ opens up an increasing number of iridium atoms on these sites so that catalysis can occur increasingly fast with increasing CO removal. Removal of about 70% of the CO ligands seems to correspond to a critical degree of unsaturation; we speculate that the remaining 30% of the CO ligands may be associated with iridium atoms located at the metal–support interface that are sterically blocked and unavailable to reactants even in the absence of CO ligands. These ideas are in need of testing.

CONCLUSIONS

$[Ir_4(CO)_{12}]$ was adsorbed intact on the surface of partially dehydroxylated γ-Al_2O_3 as shown by the results of infrared and EXAFS experiments. The clusters were characterized by infrared and EXAFS spectroscopies as they were decarbonylated to various degrees. The EXAFS data indicate that the tetrahedral metal frame was retained throughout the decarbonylation, with the average Ir–Ir first-shell coordination number being 3.0 ± 0.1, with an Ir–Ir bond distance of 2.67 ± 0.01 Å. The decarbonylation process was complete at 300°C, yielding the catalyst represented as Ir_4/γ-Al_2O_3. Treatment of this sample in CO at 150–220°C led to partial recarbonylation of the tetrairidium clusters but not to the complete regeneration of $[Ir_4(CO)_{12}]$. Hydrogen chemisorption data indicate much lower H : Ir values than are characteristic of supported metallic particles of iridium; this result and the evidence of the structure of the metal–support interface indicate that the clusters should be regarded as quasi-molecular and different from bulk metallic iridium. Hydrogenation of toluene at 60°C and 1 atm was used to quantify the catalytic performance of the supported tetrairidium clusters as a function of CO ligand removal. The turnover frequency determined per uncarbonylated iridium atom was found to be roughly independent of the

degree of decarbonylation, and the activity per total iridium atom became constant after removal of about 70% of the CO ligands.

ACKNOWLEDGMENTS

This research was supported by the National Science Foundation (Grant CTS-9617257). We acknowledge beam time and the support of the U.S. Department of Energy, Division of Materials Sciences, under Contract DE-FG05-89ER45384, for its role in the operation and development of beam line X-11A at the National Synchrotron Light Source. The NSLS is supported by the Department of Energy, Division of Materials Sciences and Division of Chemical Sciences, under Contract DE-AC02-76CH00016. We are grateful to the staff of beam line X-11A for their assistance. We also acknowledge the Stanford Synchrotron Radiation Laboratory for access to beam time on beam line 2-3. The EXAFS data were analyzed with the XDAP software developed by Vaarkamp *et al*. (10).

REFERENCES

1. Ertl, G., *in* "Metal Clusters in Catalysis" (B. C. Gates, L. Guczi, and H. Knözinger, Eds.), p. 577. Elsevier, Amsterdam, 1986.
2. Gates, B. C., *Chem. Rev.* **95**, 511 (1995).
3. Xu, Z., Xiao, F.-S., Purnell, S. K., Alexeev, O., Kawi, S., Deutsch, S. E., and Gates, B. C., *Nature (London)* **372**, 346 (1994).
4. Maloney, S. D., van Zon, F. B. M., Kelley, M. J., Koningsberger, D. C., and Gates, B. C., *Catal. Lett.* **5**, 161 (1990).
5. Maloney, S. D., Kelley, M. J., Koningsberger, D. C., and Gates, B. C., *J. Phys. Chem*. **95**, 9406 (1991).
6. Kawi, S., Chang, J.-R., and Gates, B. C., *J. Am. Chem. Soc.* **115**, 4830 (1993).
7. Jentoft, R. E., Deutsch, S. E., and Gates, B. C., *Rev. Sci. Instrum*. **67**, 2111 (1996).
8. Teo, B. K., and Lee, P. A., *J. Am. Chem. Soc.* **101**, 2815 (1979).
9. Duivenvoorden, F. B. M., Koningsberger, D. C., Uh, Y. S., and Gates, B. C., *J. Am. Chem. Soc.* **108**, 6254 (1986).
10. Vaarkamp, M., Linders, J. C., and Koningsberger, D. C., *Physica B* **209**, 159 (1995).
11. Kirlin, P. S., van Zon, F. B. M., Koningsberger, D. C., and Gates, B. C., *J. Phys. Chem*. **94**, 8439 (1990).
12. Van Zon, J. B. A. D., Koningsberger, D. C., van't Blik, H. F. J., and Sayers, D. E., *J. Chem. Phys.* **82**, 5742 (1985).
13. Adams, D. M., and Taylor, I. D., *Chem. Soc. Faraday Trans. 2* **78**, 1573 (1982).
14. Xiao, F.-S., Weber, W. A., Alexeev, O., and Gates, B. C., *in* "Proceedings, 11th International Congress on Catalysis, Baltimore." *Stud. Surf. Sci. Catal.* **101**, Part B, 1135 (1996).
15. Kip, B. J., Duivenvoorden, F. B. M., Koningsberger, D. C., and Prins, R., *J. Catal.* **105**, 26 (1987).
16. Koningsberger, D. C., and Prins, R. (Eds.), "X-Ray Absorption: Principles, Applications, Techniques of EXAFS, SEXAFS and XANES." Wiley, New York, 1988.
17. Koningsberger, D. C., *in* "Synchrotron Techniques in Interfacial Electrochemistry" (C. A. Melendres and A. Tadjeddine, Eds.), p. 181. Kluwer Academic, Dordrecht, 1994.
18. Maloney, S. D., Kelley, M. J., and Gates, B. C., *J. Organomet. Chem*. **435**, 377 (1992).
19. Kawi, S., and Gates, B. C., *Inorg. Chem*. **31**, 2939 (1992).
20. Chini, P., Longoni, G., and Albano, V. G., *Adv. Organomet. Chem*. **14**, 285 (1976).
21. Angoletta, M., Malatesta, L., and Caglio, G. L., *J. Organomet. Chem*. **94**, 99 (1975).
22. Kawi, S., Chang, J.-R., and Gates, B. C., *J. Phys. Chem*. **97**, 5375 (1993).
23. Psaro, R., Dossi, C., Fusi, A., Pergola, R. D., Garlaschelli, L., Roberto, D., Sordelli, L., Ugo, R., and Zanoni, R., *J. Chem. Soc. Faraday Trans.* **88**, 369 (1992).
24. Churchill, M. R., and Hutchinson, J. P., *Inorg. Chem*. **17**, 3528 (1978).
25. Koningsberger, D. C., and Gates, B. C., *Catal. Lett.* **14**, 271 (1992).
26. Kampers, F. W. H., and Koningsberger, D. C., *Faraday Discuss. Chem. Soc.* **89**, 137 (1990).
27. Beutel, T., Kawi, S., Purnell, S. K., Knözinger, H., and Gates, B. C., *J. Phys. Chem*. **97**, 7284 (1993).
28. Tanaka, K., Watters, K. L., and Howe, R. F., *J. Catal.* **75**, 23 (1982).
29. Chang, J. R., Gron, L. U., Honji, A., Sanchez, K. M., and Gates, B. C., *J. Phys. Chem*. **95**, 9944 (1991).
30. Gates, B. C., *in* "Catalysis by Di- and Polynuclear Metal Cluster Complexes" (R. D. Adams and F. A. Cotton, Eds.). VCH, Weinheim, in press.
31. Vaarkamp, M., Modica, F. S., Miller, J. T., and Koningsberger, D. C., *J. Catal.* **144**, 611 (1993).
32. Zhao, A., and Gates, B. C., *Langmuir* **13**, 4024 (1997).
33. Little, L. H., "Infrared Spectra of Adsorbed Species." Academic Press, New York, 1966.
34. Somorjai, G. A., "Introduction to Surface Chemistry and Catalysis." Wiley, New York, 1994.
35. Xiao, F.-S., Xu, Z., Alexeev, O., and Gates, B. C., *J. Phys. Chem*. **99**, 1548 (1995).
36. Zhang, Z., Chen, H., Sheu, L.-K., and Sachtler, W. M. H., *J. Catal.* **127**, 213 (1991).
37. Anderson, S. L., Mizushima, T., and Udagawa, Y., *J. Phys. Chem*. **95**, 6603 (1991).
38. Chang, J.-R., Koningsberger, D. C., and Gates, B. C., *J. Am. Chem. Soc.* **114**, 6460 (1992).
39. Kubo, T., Arai, H., Tominaga, H., and Kunugi, T., *Bull. Chem. Soc. Jpn*. **45**, 607 (1972).
40. Deutsch, S. E., Mestl, G., Knözinger, H., and Gates, B. C., *J. Phys. Chem*. **101**, 1374 (1997).
41. Ponec, V., and Bond, G. C., "Catalysis by Metals and Alloys." Elsevier, Amsterdam, 1995.
42. Lin, D. S., and Vannice, M. A., *J. Catal.* **143**, 563 (1993).
43. Lin, D. S., and Vannice, M. A., *J. Catal.* **143**, 554 (1993).
44. Lu, D., and Rehr, J. J., *J. Phys. (Paris) C8* **47**, 67 (1986).
45. Van Zon, F. B. M., Maloney, S. D., Gates, B. C., and Koningsberger, D. C., *J. Am. Chem. Soc.* **115**, 10317 (1993).